Supporting Information

Realizing High In-plane Carrier Mobility in N-type SnSe Crystals through Deformation Potential Modification

Haonan Shi[1], Lizhong Su[1], Shulin Bai[1,2], Bingchao Qin[1], Yuping Wang[1], Shan Liu[1], Cheng Chang[1] and Li-Dong Zhao[1]**

[1] School of Materials Science and Engineering, Beihang University, Beijing 100191, China.
[2] College of Materials Science and Engineering, Liaoning Technical University, Fuxin, Liaoning 123000, China

Corresponding Authors: changchengcc@buaa.edu.cn, zhaolidong@buaa.edu.cn

1. Experiment Details

1.1 Samples synthesis

Raw materials, including Sn (bulk, 5N), Se (shot, 4N), Pb(bulk, 5N) and $SnBr_2$(powder, 2N), were used to synthesize the series of $Sn_{1-x}Pb_xSe_{0.97}Br_{0.03}$ (x = 0, 0.02, 0.04, 0.06, 0.08, 0.10, 0.12) crystal samples. Stoichiometric amounts of high-purity raw materials were weighed and mixed into the vacuum-sealed quartz tubes. The bottom of the tubes was pointed for the growth of the seed crystal. The tubes were loaded into the verticle furnace. The middle part of the glass tube was in the heated area and the temperature of the bottom was ~ 100 K lower than the heated area, leading to a temperature gradient. The furnace was heated to ~ 1313 K for 16 h and kept for another 16 h, and then the temperature slowly dropped to ~ 1073 K with the rate of ~ 1 K h^{-1}. Finally, the furnace cooled to room temperature.

1.2 X-ray diffraction

The small piece peeled from the crystal sample along the cleavage plane, as shown in the inset of **Figure S1**, was used for phase constitution identification. The diffraction patterns were characterized by X-ray diffraction (D/MAX2200pc, Rigaku, Japan) with Cu K_α radiation (λ ~ 0.15418 nm). The measurement was conducted at 40 kV and 20 mA with a scanning speed of 6 degrees per minute.

1.3 Electrical transport properties

The *n*-type SnSe crystals were cut and polished into bars with the dimensions of ~ 3 × 3 × 10 mm3 for the measurement of Seebeck coefficient and electrical conductivity by the ZEM-3 instrument (ADVANCE RIKO, Inc., Japan). The measurements were carried out in a helium atmosphere at 300–773 K. The samples were coated with a thin layer of boron nitride to prevent possible evaporation. The uncertainty of the Seebeck coefficient and electrical conductivity measurement is within 5 %.

1.4 Thermal transport properties

The thermal conductivity was calculated by $\kappa_{tot} = D\rho C_p$. D is the thermal diffusivity, which was measured by the LFA457 instrument (Netzsch, Germany) in the nitrogen atmosphere from 300 K to 773 K. The samples for testing were the pieces cut

and polished into the size of ~ 6 × 6 × 1.5 mm^3. The density (ρ) was determined by the mass and dimensions of the sample. C_p represents the specific heat capacity estimated by the Dulong-Petit law.

1.5 Hall measurement

The carrier concentration (n_H) was calculated by $n_H = 1/(eR_H)$, where e is the electron charge and R_H is the Hall coefficient, which was measured by a Hall measurement system (Lake Shore 8400 series, USA). The crystal samples were cut and polished into pieces of ~ 8 × 8 × 0.8 mm^3 for measurement and the test temperatures were 300–773 K.

1.6 The calculation of deformation potential

The deformation potential (Ξ) was calculated by[1, 2]:

$$\Xi = \left[9\mu_W \left(\frac{T}{300} \right)^{\frac{5}{2}} T^{-1} \frac{3\pi m_I^*}{2k_B^2 \hbar C_l N_V} \right]^{-\frac{1}{2}} \text{*MERGEFORMAT(S1)}$$

where μ_W is the weighted mobility, T is the temperature, m_I^* is the inertial effective mass, k_B is the Boltzmann constant, $\hbar$ is the Reduced Planck constant, C_l longitudinal elasticity modulus calculated by $C_l = v_l^2\rho$ (v_l is longitudinal sound velocity and ρ is the density) and N_v is orbital degeneracy.

In this work, the relative deformation potential (Ξ/Ξ_0) is calculated as follows:

$$\frac{\Xi}{\Xi_0} = \left(\frac{\mu_W}{\rho v_l^2} \right)^{-\frac{1}{2}} \left(\frac{\rho_0 v_{l0}^2}{\mu_{W0}} \right)^{-\frac{1}{2}} \text{* MERGEFORMAT (S2)}$$

where the parameters with 0 as the subscript represent the data of the matrix sample (x = 0).

1.7 The detailed calculation of the single parabolic band (SPB) model

The theoretical line in **Figure 3(a)** and the Pisarenko line in **Figure 3(c)** are calculated based on the single parabolic band (SPB) model. Under the assumption of the SPB model, the Seebeck coefficient and carrier concentration is expressed as[3]:

$$S = \pm \frac{k_B}{e} \left[\frac{(r+2.5)F_{(r+1.5)}(\eta)}{(r+1.5)F_{(r+0.5)}(\eta)} - \eta \right] \text{* MERGEFORMAT (S3)}$$

$$n = \int_0^\infty f_0(E)g(E)dx = 4\pi\left(\frac{2m^* k_B T}{h^2}\right)^{1.5} F_{0.5}(\eta)$$ * MERGEFORMAT (S4)

where r is the scattering factor, $F_n(\eta)$ is the Fermi integral function, η is the reduced Fermi energy, f_0 is the equilibrium-state Fermi distribution function, and $g(E)$ is the density of the electron states near the band edge.

The effective mass of the Pb-free sample($SnSe_{0.97}Br_{0.03}$) can be calculated with the measured values of the Seebeck coefficient and carrier concentration by **Equations (S3)** and **(S4)**. And then given a series of carrier concentrations, the Pisarenko line can be described with the specific effective mass, as shown in **Figure 3(c)**.

The carrier mobility in the SPB model can be expressed by[3]:

$$\mu = \frac{2\mu_0}{3} k_B^r T^r (r+1.5)\frac{F_{r+0.5}(\eta)}{F_{0.5}(\eta)}$$ * MERGEFORMAT (S5)

where μ_0 is defined as $e\tau_0/m^*$. The μ_0 of $SnSe_{0.97}Br_{0.03}$ can be calculated with the measured carrier mobility and carrier concentration. The relationship between carrier mobility and carrier concentration, which is the theoretical line in **Figure 3(a)**, can be described by **Equations (S4)** and **(S5)**.

1.8 The detailed calculation of the Callaway model

The Callaway model is utilized to describe the effect of Pb_{Sn} point defects on the lattice thermal conductivity[4]. The ratio of the lattice thermal conductivities of the sample with point defects (κ_{lat}) and the parent material ($\kappa_{lat,\,p}$) can be expressed as[4, 5]:

$$\frac{\kappa_{lat}}{\kappa_{lat,p}} = \frac{\arctan U}{U}$$ * MERGEFORMAT (S6)

$$U = \left(\frac{\pi^2 \theta_D V \kappa_{lat,p} \Gamma}{h v_a^2}\right)^{0.5}$$ * MERGEFORMAT (S7)

where θ_D is the Debye temperature, V is the average volume per atom, h is the Planck constant, and v_a is the sound velocity. Γ is the imperfection scaling parameter representing the scattering strength of the point defects.

In SnSe, Γ is defined as:

$$\Gamma = \frac{1}{2}\cdot\frac{M_{cation}}{M}\Gamma_{cation} + \frac{1}{2}\cdot\frac{M_{anion}}{M}\Gamma_{anion} \text{ * MERGEFORMAT (S8)}$$

In this work, we alloy Pb into Sn sites and concentrate on the effect of Pb_{Sn} defects. Therefore, the imperfection scaling parameter on the anion sites (Γ_{anion}) can be regarded as zero, and the Equation (8) can be written as:

$$\Gamma = \frac{1}{2}\cdot\left(\frac{M_{cation}}{M}\right)^2\Gamma_{cation} \text{ * MERGEFORMAT (S9)}$$

where M_{cation}=(1-x)M_{Sn}+xM_{Pb}, representing the average mass of cation sites, M=(M_{Pb}+M_{Sn})/2, Γ_{cation} is the imperfection scaling parameter on the anion sites, which is defined as:

$$\Gamma_{cation} = \Gamma_{(Sn,Pb)} = \Gamma_S + \Gamma_M \text{ * MERGEFORMAT (S10)}$$

$$\Gamma_S = \varepsilon x(1-x)\left(\frac{\Delta r}{r_{(Sn,Pb)}}\right)^2 \text{ * MERGEFORMAT (S11)}$$

$$\Gamma_M = x(1-x)\left(\frac{\Delta M}{M_{(Sn,Pb)}}\right)^2 \text{ * MERGEFORMAT (S12)}$$

$$\varepsilon = \frac{2}{9}\left(\frac{6.4\gamma(1+\nu)}{1-\nu}\right)^2 \text{ * MERGEFORMAT (S13)}$$

$$\Delta r = r_{Sn} - r_{Pb} \text{ * MERGEFORMAT (S14)}$$

$$r_{(Sn,Pb)} = (1-x)r_{Sn} + xr_{Pb} \text{ * MERGEFORMAT (S15)}$$

$$\Delta M = M_{Sn} - M_{Pb} \text{ * MERGEFORMAT (S16)}$$

$$M_{(Sn,Pb)} = (1-x)M_{Sn} + xM_{Pb} \text{ * MERGEFORMAT (S17)}$$

where Γ_S and Γ_M are strain fluctuation and mass fluctuation, Δr and ΔM are the difference of radius and mass between impurity (Pb) and host atoms(Sn), r_i is the radius of the atom in its own lattice, M_i is the relative atomic mass of the atom, ε is a phenomenological adjustable parameter related to the Poisson ratio (ν) and Grüneisen parameter (γ), which are calculated by:

$$\nu = \frac{1-2\left(\frac{v_s}{v_l}\right)^2}{2-2\left(\frac{v_s}{v_l}\right)^2} \qquad \text{* MERGEFORMAT (S18)}$$

$$\gamma = \frac{3}{2}\cdot\left(\frac{1+\nu}{2-3\nu}\right) \qquad \text{* MERGEFORMAT (S19)}$$

where v_s and v_l are longitudinal and shear sound velocities, respectively.

1.9 Quasi-acoustic phonon scattering model

Under the assumption of the SPB model, the carrier mobility can be expressed as[3]:

$$\mu = \frac{2e}{3m^*}\tau k_B^r T^r \left(r+1.5\right)\frac{F_{r+0.5}(\eta)}{F_{0.5}(\eta)} \text{* MERGEFORMAT (S20)}$$

where τ is total relaxation time. For a given scattering process, the scattering factor r_0 is a constant ($r = r_0$), and the relaxation time τ_0 can also be expressed explicitly ($\tau = \tau_0$). Then, terms in **Equation (S20)** including τ, $k_B{}^r$, T^r, r+1.5 and $F_{r+0.5}(\eta)$ are all definite. That is, the carrier mobility of a material can be expressed specifically under a given scattering process.

Once another subordinate scattering process is introduced into the material, the scattering factor r and the relaxation time τ will change. Here, we assume that the relaxation time τ will vary linearly with the relaxation time of the dominant scattering τ_0, expressed as:

$$\tau = a\tau_0 \qquad \text{* MERGEFORMAT (S21)}$$

where a is a constant. Generally, the acoustic phonon scattering process governs the electrical transport, which scattering factor is -0.5 and the relaxation time can be expressed as[2]:

$$\tau_0 = \frac{h^4 \rho v_l^2}{16\sqrt{2}\pi^3 m^{*1.5}\Xi^2 k_B T} \qquad \text{* MERGEFORMAT (S22)}$$

From **Equations (S20)**, **(S21)**, and **(S22)**, we can conclude that the carrier mobility under the multiple scattering processes dominated by the acoustic phonon scattering

can be written as:

$$\mu = \frac{2e}{3m^*}\left(a\frac{h^4\rho v_l^2}{16\sqrt{2}\pi^3 m^{*1.5}\Xi^2 k_B}\cdot\frac{1}{T}\right)k_B^r T^r\left(r+1.5\right)\frac{F_{r+0.5}(\eta)}{F_{0.5}(\eta)}\backslash*$$

MERGEFORMAT (S23)

Obviously, the carrier mobility can be simplified to a function of temperature:

$$\mu = AT^{r-1} \propto T^{r-1} \qquad \backslash* \text{ MERGEFORMAT (S24)}$$

Therefore, the scattering factor under the multiple scattering processes can be obtained from the slope of lgμ-lg$T$.

1.10 The detailed first-principles calculations

All the first-principles calculations were performed with generalized gradient approximation (GGA) in combination with the projector augmented wave (PAW) method as implemented in the Vienna Ab initio Simulation Package (VASP)[6, 7]. The Perdew–Burke–Ernzerhof (PBE) functional was used to describe the exchange-correlation energy[8]. A plane wave basis with a convergence kinetic energy cut-off of 500 eV was adopted in all calculations. The Brillouin Zone (BZ) was sampled using the Monkhorst-Pack k-mesh of 4×12×12 with the energy convergence criterion of 10^{-8} eV. The crystals were fully optimized within the Hellmann-Feynman force convergence criterion of 10^{-3} eV/Å. Moment tensor potentials (MTPs) were trained as a class of accurate machine-learning interatomic potentials, which interpolates interatomic forces using the MLIP code[9]. The MTPs with an exceptionally high level of accuracy were similar to the classical potential that contains optimized parameters based on a set of training configurations[10]. To obtain training sets for MTP, Ab initio molecular dynamics (AIMD) simulations[11] based on the NVT simulation with Langevin thermostat were performed with 1ps at a time step of 1fs for the 1×4×4 ($Pb_{32}Sn_{32}Se_{64}$) and 2×2×2 ($Sn_{32}Se_{32}$) supercells at 50K, 300K, and 500K. With the premise of obtained training sets for MTPs, the phonon spectra of $PbSnSe_2$ and SnSe were evaluated using the PHONOPY code[12].

1.11 The mechanical properties calculation

The mechanical properties are calculated according to the sound velocities along

in-plane and out-of-plane directions. The Young's modulus (E) and shear modulus (G) are expressed by:

$$E = \frac{\rho v_s^2 \left(3v_l^2 - 4v_s^2\right)}{v_l^2 - v_s^2} \qquad \text{* MERGEFORMAT (S25)}$$

$$G = \frac{E}{2\left(1+\nu\right)} \qquad \text{* MERGEFORMAT (S26)}$$

where ν is the Poisson ratio obtained from **Equation S18**.

2. Supporting Figures and Tables

Figure S1:

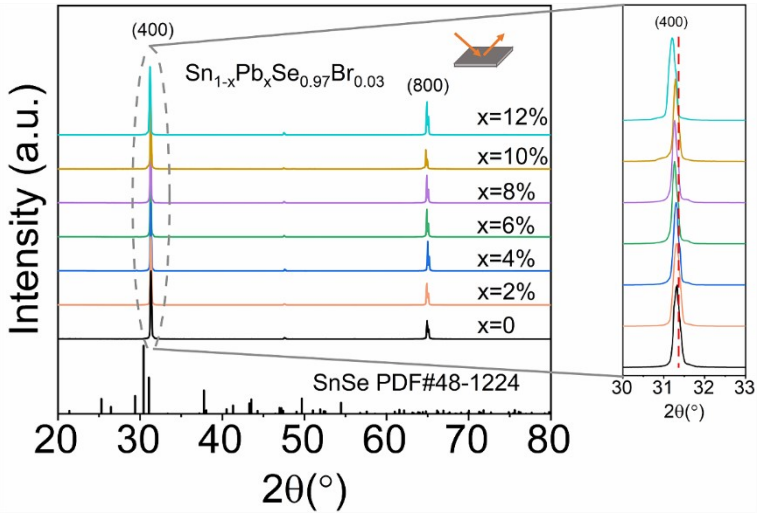

Figure S1. The X-ray diffraction of $Sn_{1-x}Pb_xSe_{0.97}Br_{0.03}$ (x = 0, 0.02, 0.04, 0.06, 0.08, 0.10, 0.12) crystals on the (400) cleavage plane. The peaks shift to the left due to the Pb alloying.

Figure S2

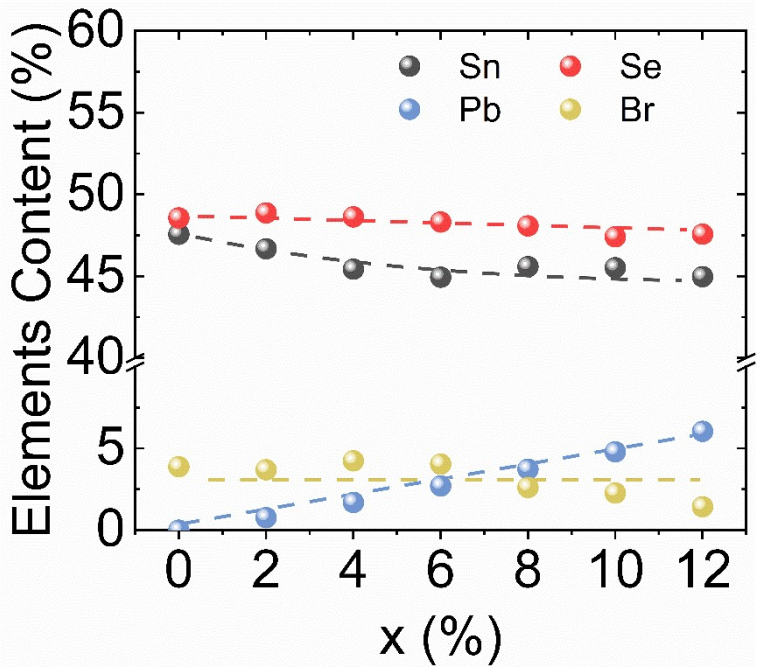

Figure S2. The compositions of $Sn_{1-x}Pb_xSe_{0.97}Br_{0.03}$ (x = 0, 0.02, 0.04, 0.06, 0.08, 0.10, 0.12) samples measured by EDS. The fluctuation of Br content is disturbed by the Al-based sample holder.

Figure S3

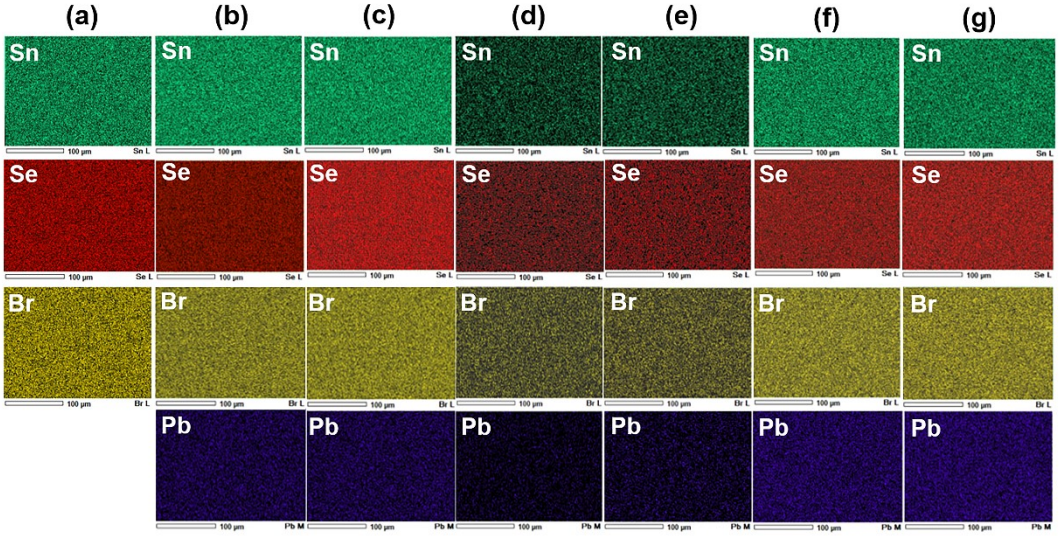

Figure S3. The energy dispersive spectrometer (EDS) mapping images of different elements in $Sn_{1-x}Pb_xSe_{0.97}Br_{0.03}$ (x = 0, 0.02, 0.04, 0.06, 0.08, 0.10, 0.12) samples. (a)-(g) represent the Pb content of 0, 0.02, 0.04, 0.06, 0.08, 0.10, 0.12, respectively.

Figure S4:

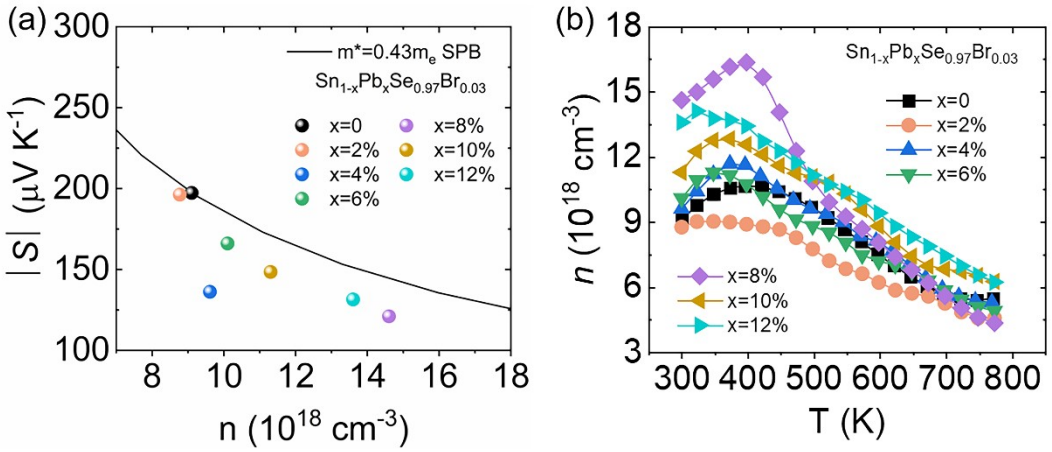

Figure S4. (a) The Pisarenko relationship of Pb-alloyed *n*-type SnSe crystals without considering the scattering factor based on the SPB model; (b) the carrier concentration as a function of temperature.

Figure S5

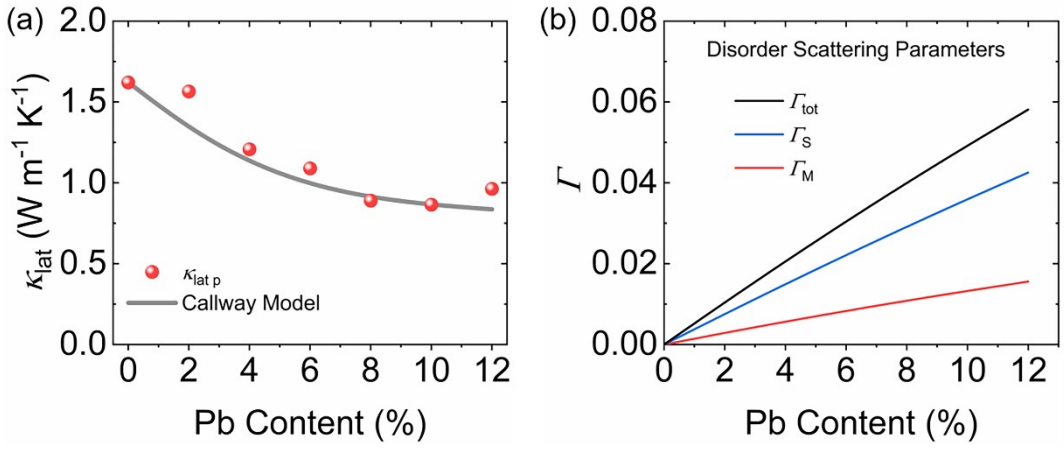

Figure S5. (a) Lattice thermal conductivity at 300 K as a function of Pb content and Callaway model simulation; (b) the effect of mass and strain fluctuation on thermal conductivity.

Figure S6

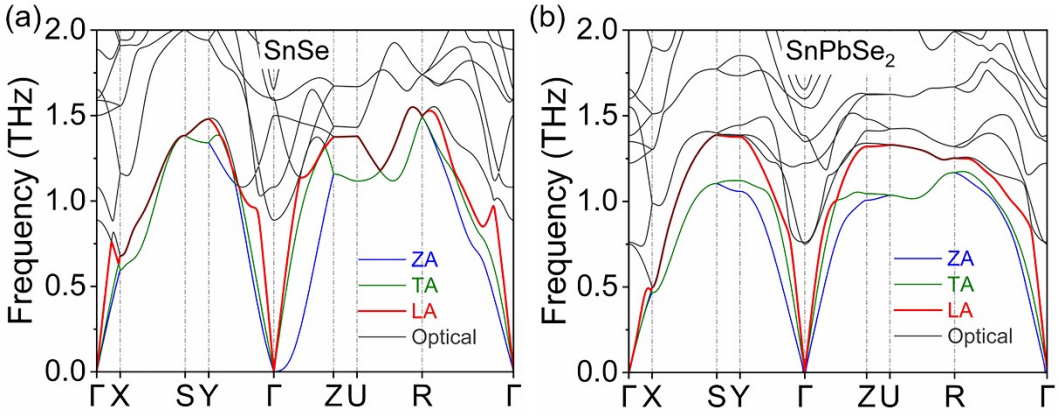

Figure S6. The DFT calculated phonon dispersions of (a) SnSe and (b) $SnPbSe_2$.

Figure S7

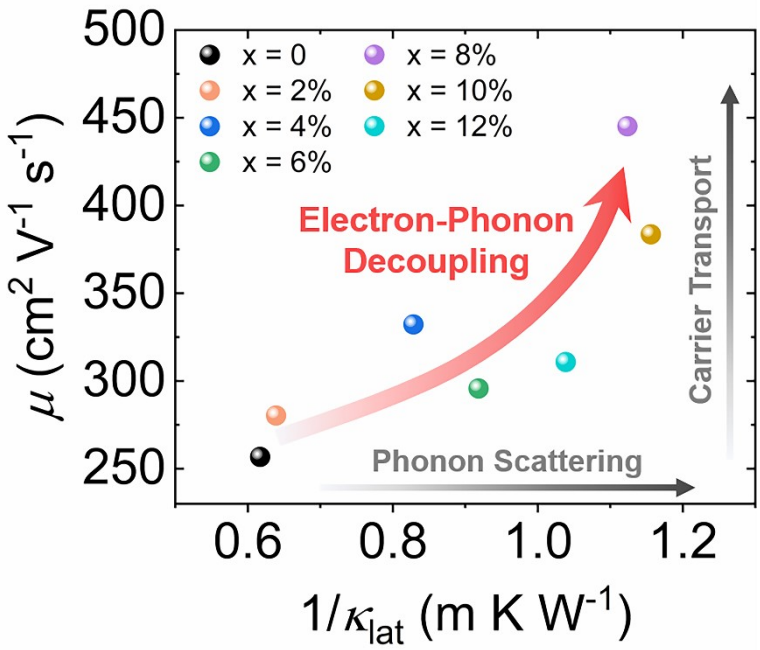

Figure S7. The synergistic optimization of carrier mobility and lattice thermal conductivity in $Sn_{1-x}Pb_xSe_{0.97}Br_{0.03}$ (x = 0, 0.02, 0.04, 0.06, 0.08, 0.10, 0.12) samples.

Figure S8:

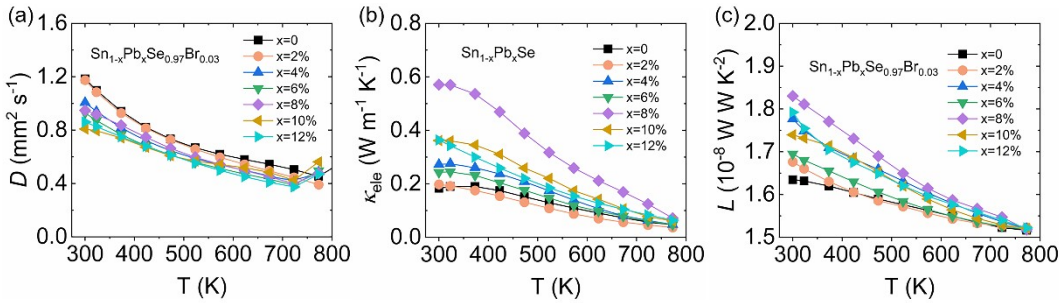

Figure S8. The thermal transport parameters of Pb-alloyed *n*-type SnSe crystals: (a) thermal diffusion; (b) electronic thermal conductivity; (c) Lorenz constant.

Figure S9

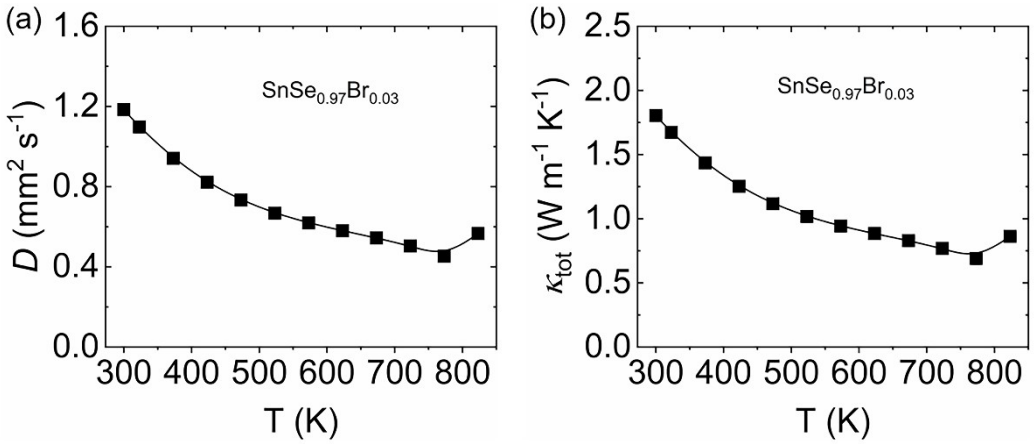

Figure S9. The thermal transport properties of $SnSe_{0.97}Br_{0.03}$: (a) thermal diffusion; (b) total thermal conductivity. The text temperature is extended to 823 K to show the phase transition of the Pb-free SnSe crystal.

Figure S10:

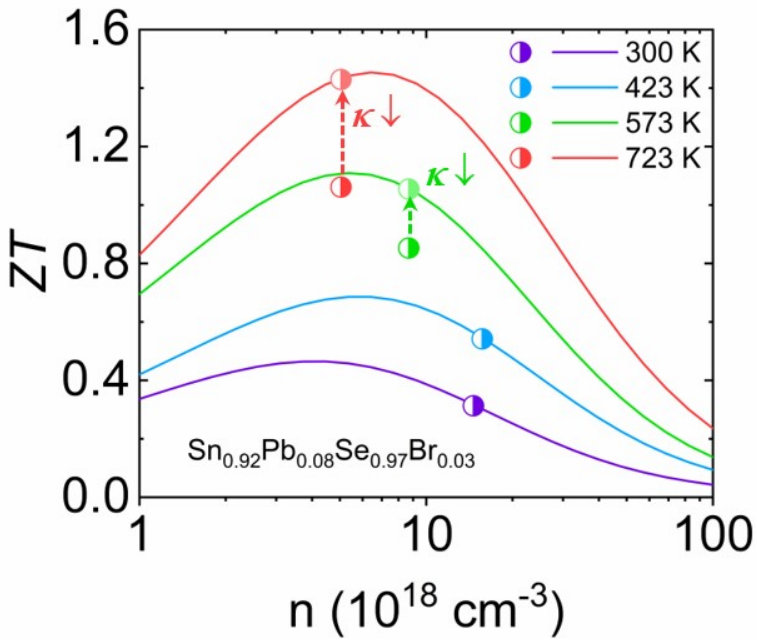

Figure S10. The prediction of *ZT* value based on the single parabolic band model.

Figure S11:

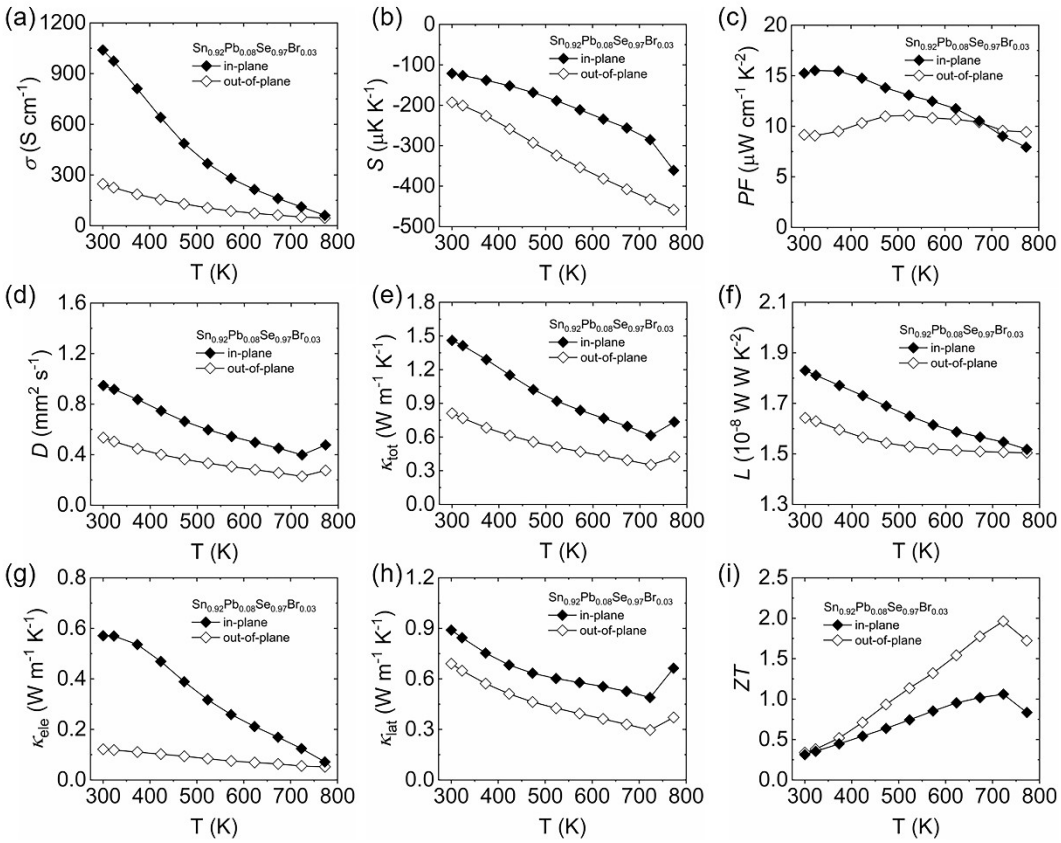

Figure S11. The thermoelectric properties of the best-optimized sample $Sn_{0.92}Pb_{0.08}Se_{0.97}Br_{0.03}$ along in-plane and out-of-plane directions as functions of temperature: (a) electrical conductivity; (b) Seebeck coefficient; (c) power factor; (d) thermal diffusion; (e) total thermal conductivity; (f) Lorenz constant; (g) electronic thermal conductivity; (h) lattice thermal conductivity; (i) *ZT* value.

Table S1

Table S1. The mechanical properties of SnSe crystal ($SnSe_{0.97}Br_{0.03}$) along in-plane and out-of-plane directions.

Directions	In-plane	Out-of-plane
Longitudinal Sound Velocity ($m\ s^{-1}$)	4487.18	2184.12
Shear Sound Velocity ($m\ s^{-1}$)	3625.48	1960.79
Young's Modulus (GPa)	77.58	60.14
Shear Modulus (GPa)	28.84	23.25

Table S2

Table S2. The nominal and practical compositions of $Sn_{1-x}Pb_xSe_{0.97}Br_{0.03}$ (x = 0, 0.02, 0.04, 0.06, 0.08, 0.10, 0.12) samples.

x	Nominal Compositions (%)				Practical Compositions (%)			
	Sn	Pb	Se	Br	Sn	Pb	Se	Br
0	50	0	48.5	1.5	47.56	0	48.56	3.88
0.02	49	1	48.5	1.5	46.67	0.77	48.87	3.69
0.04	48	2	48.5	1.5	45.43	1.70	48.63	4.24
0.06	47	3	48.5	1.5	44.94	2.71	48.31	4.04
0.08	46	4	48.5	1.5	45.58	3.73	48.08	2.61
0.10	45	5	48.5	1.5	45.52	4.79	47.41	2.27
0.12	44	6	48.5	1.5	44.97	6.04	47.57	1.43

Table S3:

Table S3. The longitudinal and shear sound velocity in different Pb content samples.

Pb Content (%)	Longitudinal Sound Velocity ($m\ s^{-1}$)	Shear Sound Velocity ($m\ s^{-1}$)
0	4487.18	2184.12
2	4216.72	2092.04
4	3618.09	2084.48
6	3978.26	2096.06
8	3463.41	1953.69
10	3561.22	1979.24
12	3795.18	2034.17

Table S4:

Table S4. The densities of the different Pb content samples.

Pb Content (%)	Density (g cm^{-3})
0	6.05
2	6.00
4	5.94
6	5.85
8	6.34
10	6.30
12	6.45

Reference

1. L. Su, D. Wang, S. Wang, B. Qin, Y. Wang, Y. Qin, Y. Jin, C. Chang and L. D. Zhao, *Science*, 2022, **375**, 1385-1389.
2. J. Bardeen and W. Shockley, *Phys. Rev.*, 1950, **80**, 72-80.
3. L. Su, H. Shi, S. Wang, D. Wang, B. Qin, Y. Wang, C. Chang and L.-D. Zhao, *Adv. Energy Mater.*, 2023, **13**, 2300312.
4. J. Callaway and H. C. v. Baeyer, *Phys. Rev.*, 1960, **120**, 1149-1154.
5. C. L. Wan, W. Pan, Q. Xu, Y. X. Qin, J. D. Wang, Z. X. Qu and M. H. Fang, *Phys. Rev. B*, 2006, **74**, 144109.
6. P. E. Blochl, *Phys. Rev. B*, 1994, **50**, 17953-17979.
7. J. Hafner, *J. Comput. Chem.*, 2008, **29**, 2044-2078.
8. Z. Wu and R. E. Cohen, *Phys. Rev. B*, 2006, **73**, 235116.
9. I. S. Novikov, K. Gubaev, E. V. Podryabinkin and A. V. Shapeev, *Mach. Learn. Sci. Technol.*, 2021, **2**, 025002.
10. E. V. Podryabinkin, E. V. Tikhonov, A. V. Shapeev and A. R. Oganov, *Phys. Rev. B*, 2019, **99**, 064114.
11. M. E. Tuckerman, P. J. Ungar, T. v. Rosenvinge and M. L. Klein, *J. Phys. Chem.*, 1996, **100**, 12878–12887.
12. A. Togo and I. Tanaka, *Scr. Mater.*, 2015, **108**, 1-5.